

# Interaction of Mechanics and Electrochemistry for Magnesium Alloys

En-Hou Han<sup>†</sup>, Jianqiu Wang, and Wei Ke

*Institute of Metal Research, Chinese Academy of Sciences, China*

Magnesium alloys become popular research topic in last decade due to its light weight and relatively high strength-to-weight ratio in the energy aspiration age. Almost all structure materials are supposed to suspend stress. Magnesium is quite sensitive to corrosive environment, and also sensitive to environmental assisted cracking. However, so far we have the limited knowledge about the environmental sensitive cracking of magnesium alloys.

The corrosion fatigue (CF) test was conducted. Many factors' effects, like grain size, texture, heat treatment, loading frequency, stress ratio, strain rate, chemical composition of environment, pH value, relative humidity were investigated. The results showed that all these factors had obvious influence on the crack initiation and propagation. Especially the dependence of CF life on pH value and frequency is quite different to the other traditional structural metallic materials.

In order to interpret the results, the electrochemistry tests by polarization dynamic curve and electrochemical impedance spectroscopy were conducted with and without stress. The corrosion of magnesium alloys was also studied by in-situ observation in environmental scanning electron microscopy (ESEM). The corrosion rate changed with the wetting time during the initial corrosion process. The pre-charging of hydrogen caused crack initiated at  $\beta$  phase, and with the increase of wetting time the crack propagated, implying that hydrogen produced by corrosion reaction participated in the process.

**Keywords** : corrosion fatigue, stress corrosion cracking, magnesium alloys, crack initiation, crack propagation, frequency, pH value

## 1. Introduction

Magnesium alloys serve increasingly as structural components in automobile and aircraft industry due to its relatively high strength-to-weight ratio and excellent technological properties. Since many mechanically loaded parts are often subjected to prolonged cyclic stresses in an active medium, it is of significant scientific and practical interest to study corrosion fatigue (CF) of magnesium alloys. The fatigue life of magnesium alloys in corrosive solutions is always less than that in air. The poor corrosion resistance of magnesium and its alloys restrict their wide application. In the past decade, many research works had concentrated on the effects of microstructure and environmental factors on the corrosion behavior of magnesium and its alloys.<sup>1-15)</sup>

Atmospheric corrosion is one of the typical interfacial phenomena, which includes physical, chemical, biological and statistical phenomena on the boundary of multiphase. In the atmospheric corrosion of metals such as pure magnesium and its alloys, the surfaces are usually covered by

droplets or a thin water film due to the frequent rainfall, dew condensation and snow thaw, which indicates that the surfaces experience wetting and drying cycles with different periods. Therefore, the changes of surface states such as the formation and spreading of micro-droplets and formation of water film are vital for the initial atmospheric corrosion. In solutions, the Mg alloys have different corrosion behaviors due to its negative difference effect. Hydrogen evolution, aggressive species content, temperature have big effect on corrosion fatigue behaviors of magnesium alloys. Eliezer and Gutman et al<sup>16,17)</sup> carried out corrosion fatigue tests on extruded AZ31, AZ91, AM50, and ZK60 magnesium alloys in air, NaCl and borate solutions. Their results indicated that under the same stress, the corrosion fatigue life of extruded alloys is significantly longer than that of die-cast alloys. Dietzel et al<sup>18)</sup> studied the stress corrosion cracking (SCC) behavior of AZ31 magnesium alloy under slow strain rate tensile tests and their results showed that the AZ31 sheet material is susceptible to SCC in distilled water, ASTM D1387 solution, 0.01 M NaCl and 0.1 M NaCl solution. It is proposed that hydrogen embrittlement is the mechanism for

<sup>†</sup> Corresponding author: ehhan@imr.ac.cn

the SCC. Although the interaction of mechanics and electrochemistry is an important issue for the application of magnesium alloys, until now there is no enough research work on this subject. This paper aimed to reveal the corrosion mechanism of magnesium alloy in wet air and solutions and the interaction of corrosion and stress of magnesium alloys.

In recent years, laser microscope and optical microscope have been used to study the formation and spreading of micro-droplets around the preferential added solutions. But these equipments are limited to low magnification, which can not study the influences of microstructure in detail such as grain boundary, secondary phases, defects, scratches and etc. on the formation and spreading of micro-droplets. The formation and spreading of micro-droplets which formed around the preferential added solutions can not be accurately reflected the actual formation and spreading of micro-droplets on the fresh sample surfaces due to the disturbance of surface integrality by preferential added solutions and ignoring influences of microstructure. Moreover, the changes of surface status that were parallel to the formation and spreading of micro-droplets, and the influences of corrosion products also can not be reflected with the increasing of wetting time. ESEM chamber environments can be continuously controlled, which can provide the same dewing environment for the whole sample surface to guarantee the surface integrality. Moreover, the influences of microstructure and the corrosion products formed during the formation and spreading of micro-droplets are evident, which is close to actual atmospheric corrosion medium. In addition, the average surface corrosion status at different wetting time can be quantitatively and continuously illustrated.

Magnesium can quickly develop an oxide film on the surface in air, but magnesium oxide (MgO) with the Pilling-Bedworth ratio of 0.81 can only provide limited protection. In wet air and aqueous solutions, oxide and hydroxide layers (MgO/Mg(OH)<sub>2</sub>) can form spontaneously on the surface. According to Schmutz et al.,<sup>7)</sup> Mg(OH)<sub>2</sub> has the Pilling-Bedworth ratio of 1.77. The film can not provide enough protection. Both pure magnesium and its alloys have poor pitting resistance in aqueous solution containing aggressive anions.<sup>14)</sup> The oxide and hydroxide films tend to break down chemically in the solution containing chloride, sulfate and bromide. The corrosion film of AZ91 in Na<sub>2</sub>SO<sub>4</sub> solution with time has been studied using electrochemical impedance spectroscopy (EIS) and environmental scanning electron microscopy (ESEM) in this paper. It was found that pre-charging hydrogen could crack β phase of AZ91, which would assist SCC and CF of magnesium alloys. The influence of temperature, rela-

tive humidity and the solution concentration on corrosion fatigue performance of magnesium alloys were also studied in this paper.

## 2. Experiment

The materials studied were pure magnesium, as-cast AZ91 magnesium alloy, AZ61 extruded sheet and AZ31B rolled sheet. The chemical composition of pure magnesium (wt. %) was <0.003Al, <0.005Zn, 0.005Mn, <0.005Ni, 0.01Fe, <0.003Cu and balance Mg. As-cast AZ91 alloy was 9.14 Al, 0.49Zn, 0.26Mn, <0.001Ni, 0.002Fe, 0.002 Cu and balance Mg. AZ61 alloy was 6.6Al, 0.17Mn, 0.45Zn, and balance Mg extrusion sheet and its 0.2% yield strength (YS), ultimate tensile strength (UTS) and elongation to rupture (E<sub>r</sub>) were 187 MPa, 274 MPa, and 21% respectively. AZ31B was 3.20%Al, 0.45%Zn, 0.26%Mn, 0.15%Si, 0.03%Cu and Mg balance. Its yield strength, ultimate tensile strength, elongation to fracture are 135 MPa, 250 MPa, 19.5% respectively.

The AZ91 samples were cut into cylinder by 8mm in diameter. The surface was polished using 1000, 2000 grit silicon carbide papers and then fine polished using 0.5 μm diamond paste, cleaned with distilled water and acetone, and dried in cool air. Then the mechanically polished samples were electro-polished in 60 ml 60% perchloric acid, 140 ml water and 800 ml 95% ethanol solution for several seconds.

In-situ observations of the initial corrosion for pure magnesium and AZ91 magnesium alloy under cyclic wet and dry conditions were carried out using a Philips XL30 ESEM. The Energy dispersive X-ray spectroscopy (EDS) was used to measure the oxygen concentration on the sample surface when the samples were dry after each cycle. The corrosion morphologies of the selected positions were recorded during the wet and dry cycles in the gas mode using gaseous secondary electron detector (GSED). X-ray photoelectron spectroscopic (XPS) analyses were carried out using ESCALAB 250. The electrochemical impedance of AZ91 alloy in sodium sulfate solution was measured using EG&G 273 potentiostat up to 480h immersion time. The corrosion products at various immersion times were analyzed by SEM, EDS, XRD and XPS.

The samples were cathodically charged and prepared for SIMS and Mott-Schottky tests by galvanostatic polarization at 50 mA for 3h. Some charged samples, which were prepared for SIMS tests, were vacuum annealed at 150°C, 350°C and 480°C respectively for 2h. Then they were polished with 0.5 μm oil-based paste, cleaned with acetone, and then dried in cold air (During this process, the sample never contacted with water to avoid the decom-

position of hydride in case hydride formed at interior of matrix).

Fatigue tests of AZ61 were performed at ambient temperature and elevated temperature in laboratory or moist air. The single-edge, notched tension plate specimens (200 mm long and 32 mm wide with an edge notch 3.5 mm deep) was used for the fatigue crack propagation (FCP) test. The surfaces of the specimens were polished with 1000 grade silicon carbide papers. Specimens were cycled under axial tension-compression loading with a sinusoidal waveform at a cyclic frequency of 1 Hz. The stress ratio of 0 was kept constant during each individual test. Tests were carried out at room temperature (RT) (16-20°C, 40-70% RH) in ambient and warm air (temperature 60°C or 120°C). The temperature can be adjusted automatically, and the precision was 2°C. The RH was kept constant using a saturated vapor atmosphere in a completely closed chamber, and it was measured that the RH reached 100%. All tests were operated using an EHF-EB10-20L servo-hydraulic fatigue test machine.

Fatigue specimens of AZ31B with 12 mm width, 30 mm gauge length and 4 mm thickness were machined from the as-received plate so that their axes are parallel to the rolling direction. Corrosion fatigue tests of AZ31B ( $R=0.1$ ) in NaCl solution were performed using servo-mechanical testing machine (Instron model 8562). Tests were conducted under load-controlled mode with a frequency of 1.0 Hz. The maximum stress was 90% of the yield strength. The composition of electrolyte was 0.01%, 0.1%, 1% and 3.5% NaCl respectively. The solution was prepared from analytical grade NaCl and distilled water. Acoustic emission (AE) was monitored with DiSP digital acoustic emission system by PAC with a total system gain of 100 dB and a fixed signal threshold at a level of 30 dB. The preamplifiers had a 40 dB gain. Two sensors with a 20-1000 KHz bandpass filter were attached directly to the specimen using silicon grease to ensure a good acoustic connection during the test.

### 3. Results and discussion

#### 3.1 Corrosion of Mg alloys

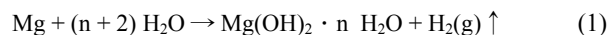
##### 3.1.1 Wet-dry cyclic corrosion

The initial corrosion process of metal in atmospheric environment has been seldom studied and usually neglected. This work showed the formation and spreading of the micro-droplets on the fresh metal surface in detail.<sup>19),20)</sup> During the first wet cycle, there were several micro-droplets on the fresh metal surface in 1 min as shown in Fig. 1(a); the micro-droplets almost covered the whole surface in 10 min as shown in Fig. 1(b); and the

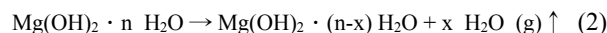
micro-droplets spread to connect to larger droplets as shown in Fig. 1(c). After the first wet cycle, the fresh metal surface was covered by corrosion products. At the second wet cycle, the appearance of droplets on the surface in 2 min was similar to that at the end of the 1st cycle. It took shorter time, only 2 min, for the formation and spreading of the micro-droplets during the second wet cycle, which indicates the corrosion products were more hydrophilic than the fresh metal surface and stimulated the formation and spreading of the micro-droplets. With the increase of the wet cycles, the water sorption became easier and at the end of 7th wet cycle a water film formed on the surface.

The preferential formed micro-droplets acted as an anode while the subsequent formed micro-droplets and wet area became cathodic. Therefore, the corrosion at the area covered by preferential formed droplets became more serious, where took on black in SE mode. It was confirmed by the *in-situ* observations in Fig. 1. Moreover, the potential between the grain boundary and the inner grain was much larger than that between the micro-droplets owing to the accumulation of Fe, Cu and Ni. So the corrosion at the grain boundary occurred rapidly when the micro-droplets formed, which was also evident in Fig. 1.

During the wet-dry cyclic test, reaction (1) happened during wet cycles, which caused the increase of the oxygen concentration:



and reaction (2) happened during dry cycles, which caused the decrease of the oxygen concentration:



Reactions (1) and (2) influence the oxygen concentration on the surface, which might result in its oscillations during tests. Once  $\text{Mg}(\text{OH})_2$  formed on the surface, which would promote the pH of micro-droplets causing the alkalization, first it could retarded the serious corrosion of magnesium, secondly according to the *in-situ* observation the formation of corrosion product assisted the water sorption.

The evolution of oxygen concentration,  $C_o$ , on the specimen surface with the wetting time is illustrated in Fig. 2. The  $C_o$  generally increased with the increasing wetting time. But the change rate of oxygen concentration with time,  $dC_o/dt$ , decreased at the first four cycles, and then oscillated with the increase of the wetting time. It meant that the corrosion process was slowed down by the corrosion products and the water sorption did not increase the corrosion rate at the initial corrosion process.

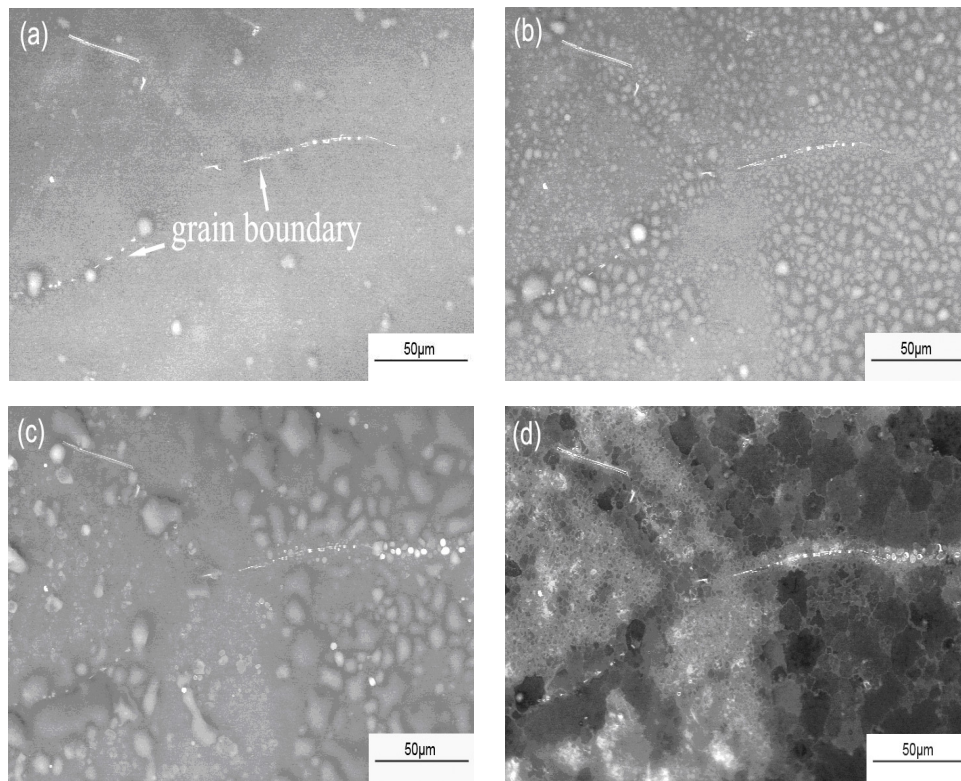


**Fig. 1.** Evolution of the micro-droplets on the surface during the first cycle at 20 MPC at the wetting time: (a) 1 min; (b) 10 min; (c) 20 min; and (d) the corrosion morphology at the end of the first cycle.

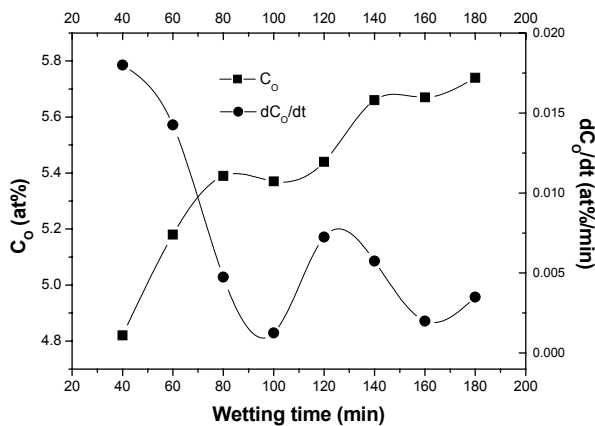


**Fig. 2.** Evolution of  $C_O$  and  $dC_O/dt$  of pure magnesium with the wetting time at 20 MPC

### 3.1.2 Corrosion in solution

The morphologies of surface and the EIS were shown in Figs. 3 & 4. When the immersion time was short, for example, 1h, the corrosion products were mainly  $Mg(OH)_2$  and  $MgAl_2(OH)_8 \cdot H_2O$ , which had not completely covered the whole surface.<sup>21),22)</sup> When the immersion time was above 1h, the corrosion products were thickened. In the

meantime, the aluminum ions concentration promoted due to the dissolution of primary  $\alpha$ -Mg phase and  $\beta$  phase, the  $MgAl_2(SO_4)_4 \cdot 2H_2O$  particles began to precipitate preferentially at some areas and a corrosion film formed on the surface, which was embodied on EIS diagram where the inductive loop at low-frequency (LF) range disappeared. With the increasing immersion time, the film was thickened and particles spread, which were evident in Fig. 2. So it was embodied on EIS diagram where the capacitive loop at medium-frequency (MF) range increased with the immersion time. In this process, some precipitates could be buried in the corrosion film, which was confirmed by the cross section observations. When the immersion time came to 181 h, pitting experienced a long incubation time, and occurred, which was embodied in EIS diagram that the capacitive loop at MF range degenerated, and the inductive loop at LF range reappeared in Fig. 4b. With the increasing immersion time, localized corrosion controlled by the precipitation of  $MgAl_2(SO_4)_4 \cdot 2H_2O$  developed both in depth and in transverse while the other regions controlled by the formation of  $Mg(OH)_2$  thickened. So the precipitates at local corroded area abnormally grew up that caused the increase of the inductance,  $L$ , which was obvious in Fig. 4.

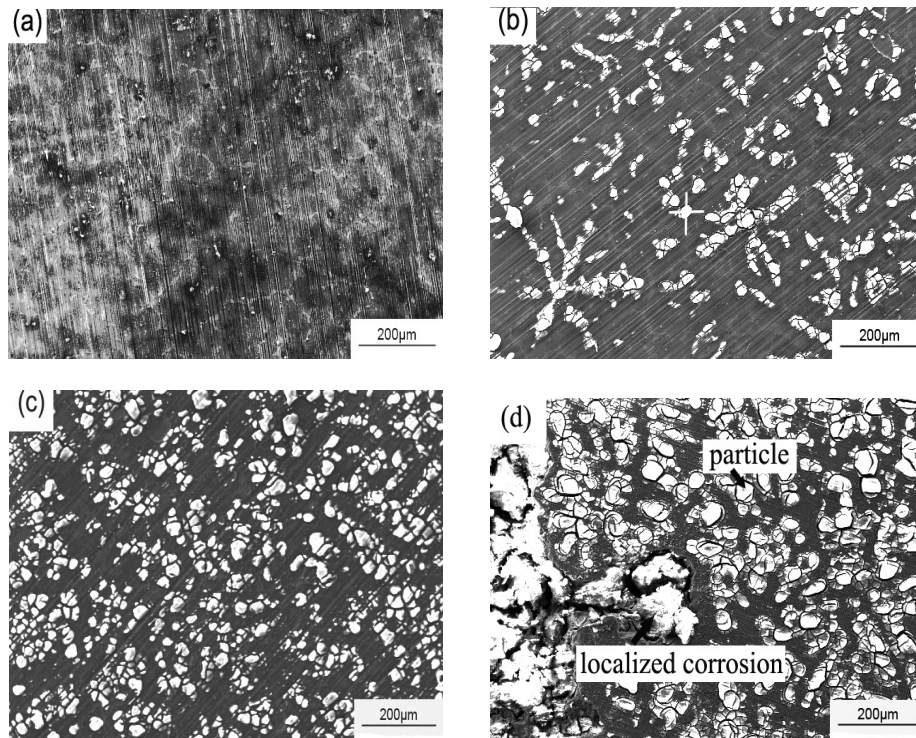


**Fig. 3.** Corrosion morphologies of AZ91 alloy after immersion in 0.1M Na<sub>2</sub>SO<sub>4</sub> solution with SEI detector for (a) 4h, (b) 48h, (c) 181h, and (d) 480h

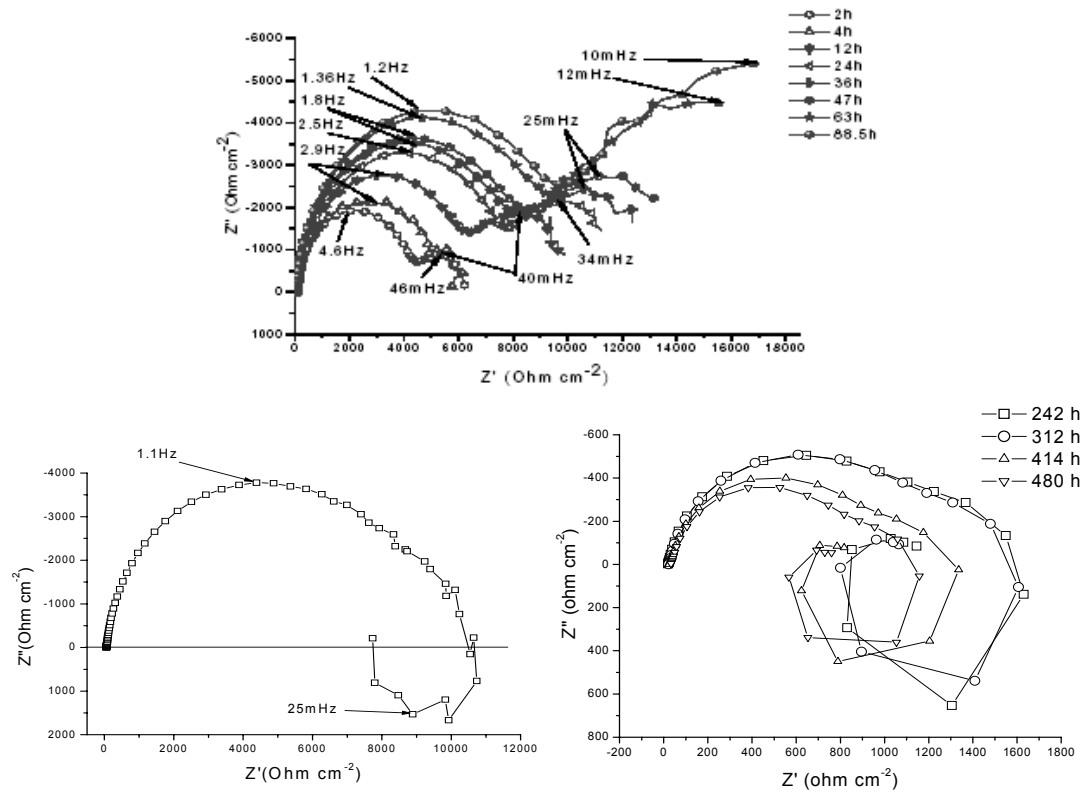


**Fig. 4.** Nyquist diagrams for AZ91 alloy at  $E_{corr}$  in 0.1 M Na<sub>2</sub>SO<sub>4</sub> solution for immersion time between 2h and 480h

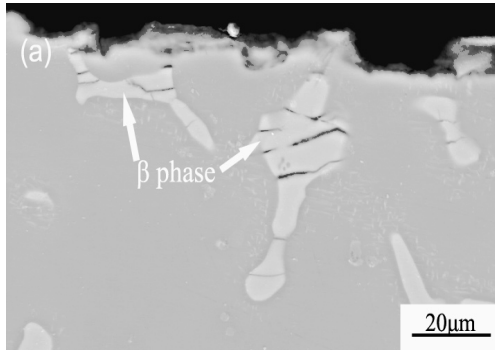


**Fig. 5.** Cross sections of AZ91 magnesium alloy in 0.1M Na<sub>2</sub>SO<sub>4</sub> solution: (a) after charging at 50 mA for 3h

### 3.1.3 Pre-charging of hydrogen

When the AZ91 magnesium alloy was immersed or cathodic charged, hydrogen atom diffused to interior, of course, including  $\beta$  phase, and preferentially formed magnesium hydride to cause the expansion of lattice. Owing to the incoherence of hydride and  $\beta$  phase, part hydrogen atoms might combine into hydrogen gas at the interfaces of hydride and  $\beta$  phase, which was another factor for the cracking of  $\beta$  phase. As a result, the synthetical effects, hydrogen pressure and expansion stress of formation of magnesium hydride, were proposed for the cracking of  $\beta$  phase during immersion and cathodic charging.

## 3.2 Corrosion fatigue of Mg alloys

### 3.2.1 Effect of temperature

The FCP rate for AZ61 shows no evident difference between RT and 60°C (Fig. 6), but it increases at least two fold at 120°C compared with RT, and the curves are zigzagged, especially at 120°C.<sup>23)</sup> Fatigue of magnesium alloys at elevated temperature is proposed to be creep fatigue. The alloy is subjected to interaction between creep load and cyclic stresses at elevated temperatures.

Figs. 7a and 7b, 7c are the optical microstructures after

fatigue at elevated temperature 60°C and 120°C, respectively. Discontinuous precipitation of  $\beta$  phase at different directions can be observed in Fig. 7b, and it possible for grain boundaries to migrate as indicated by the arrow in Fig. 7c. The substantial amount of discontinuous precipitation in AZ61 promotes creep deformation.

### 3.2.1 Effect of relative humidity

The high relative humidity can improve the fatigue crack propagation (FCP) rates in moist air as shown in Fig. 8. The FCP rates near the threshold stress intensity factor range aren't changed.<sup>24)</sup>

Hydrogen embrittlement (HE) or hydrogen induced cracking (HIC) may be the main reason why magnesium alloys accelerates their fatigue crack propagation rates in moist air. So far, three mechanisms of HE were proposed.<sup>25)</sup> The first is that hydrogen ions diffuse into metal and then coalescence in existing voids, and continuous diffusion increases the pressure on these voids. Thus, crack initiations were speeded up. The second is that diffusion of hydrogen reduced the surface energy ahead of the crack, and facilitated the FCP rates. The third is that the diffusion rates of hydrogen controls the formation process of voids,

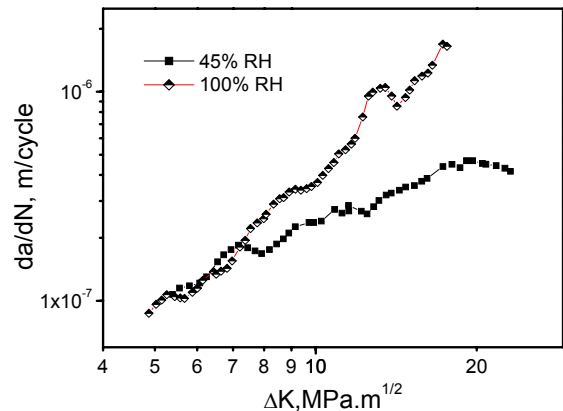


**Fig. 8.** Effect of relative humidity on FCP rates for AZ61

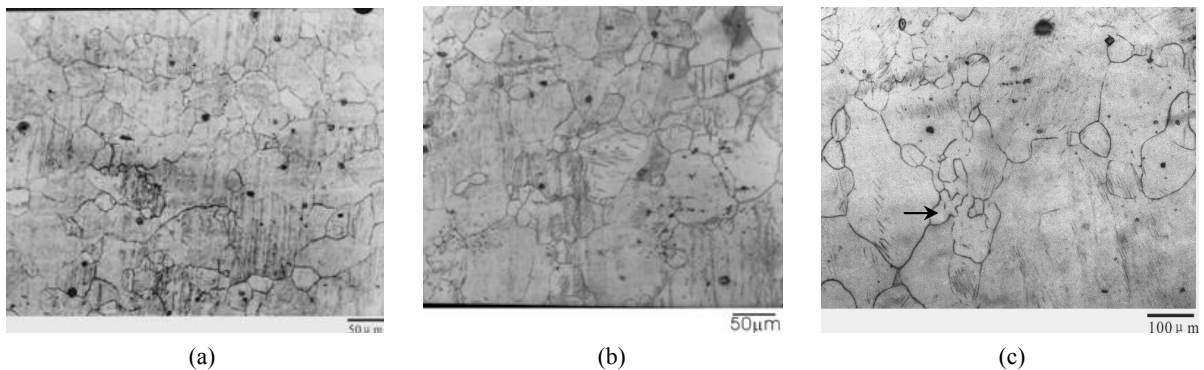


**Fig. 7.** Optical microstructure after fatigue at elevated temperature 60°C(a) and 120°C(b, c), respectively.

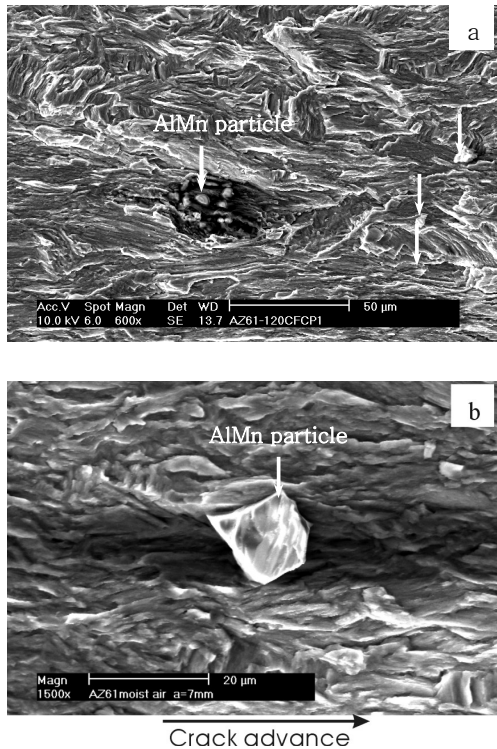


Fig. 9. Fracture morphology of AZ61 at 120°C(a ), RT in 100%RH (b )( $\Delta K=4.9\text{MPa}\cdot\text{m}^{1/2}$ )

by controlling the coalescence of voids induced by dislocation motion.

### 3.2.2 Effect of AlMn particles

The fracture morphology of AZ61 at 120°C and RT with 100%RH is shown in Fig. 9. It has the characteristic of cleavage fracture. It is obvious that AlMn particles are exposed on the fracture surface. Secondary cracks paralleled to the fatigue crack direction and voids produced by AlMn particles as indicated by the arrows shown in Fig. 9. These indicate that AlMn particles play an important role in fatigue, and speed probably the FCP rates.

As shown in Fig. 10, fatigue lifetime for as-rolled AZ31B in NaCl aqueous solution decreased with the increase of the chloride ion concentration. When the solution concentration changed from 0.1% to 1%, the fatigue lifetime curve changed sharply and the mean lifetime decreased from 30199 cycles to 4777cycles.

The evolution of cumulative AE energy as a function of time (i.e. fatigue cycles,  $f=1\text{Hz}$ ) recorded for different solution concentration had similar characteristic. Plots recorded for tests conducted in 3.5%NaCl and in 1%NaCl solution are given in Fig. 11. There are three obvious stages of AE energy during fatigue, which corresponded to crack initiation, slow crack propagation and rapid crack propagation, respectively.

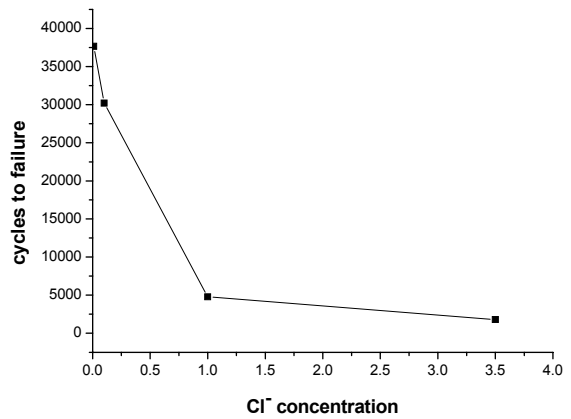
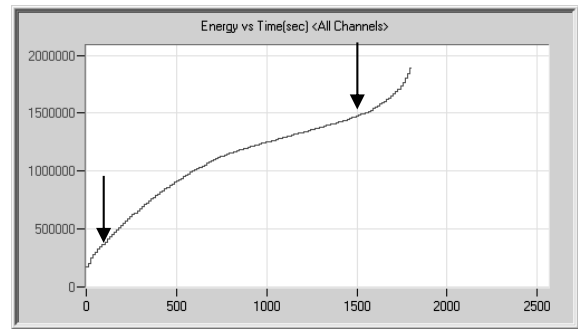
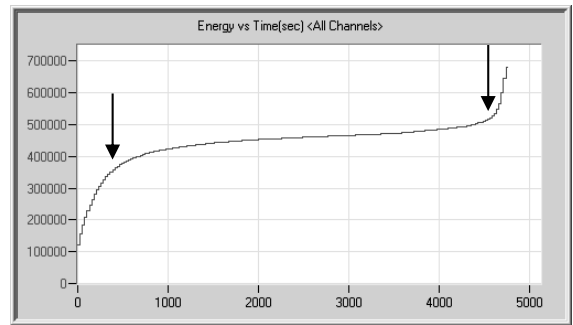


Fig. 10. Effect of Cl<sup>-</sup> concentration on fatigue lifetime for as-rolled AZ31B



(a)



(b)

Fig. 11. Cumulative plot of AE energy (a) in 3.5%NaCl, (b) in 1%NaCl

The macroscopic fracture surfaces of the samples were observed carefully after fatigue testing. Each fracture surface illustrates cracks initiated from corrosion pits. All fracture surfaces have three obvious regions with different morphology feature, that is crack origin area (region 1), stable crack propagation area (region 2) and rapid crack propagation area (region 3), as shown in Fig. 12. With the increase of Cl<sup>-</sup> concentration, the area of stable crack propagation decreased and the area of rapid crack prop-

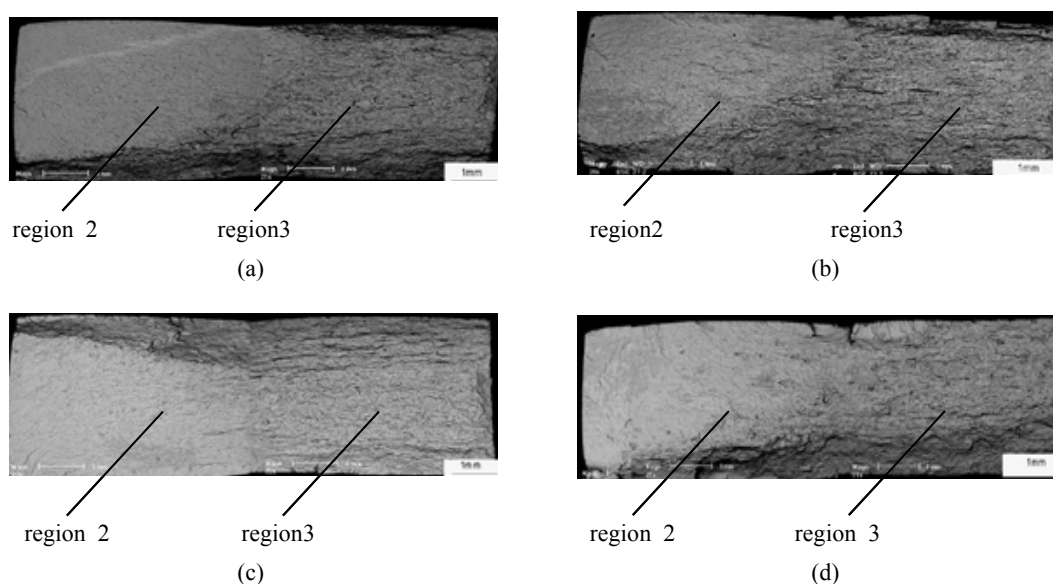


**Fig. 12.** Overall fracture surfaces of indicating the different regions inspected with backscatter SEM In (a) 0.01%NaCl; (b) 0.1%NaCl; (c) 1%NaCl; and (d) 3.5%NaCl

agation increased (Fig. 12).

### 3.3 Stress corrosion cracking and environmental effects

Slow strain rate ( $1 \times 10^{-6}$  mm/s) test results on AZ91D alloy indicated that the mechanical strength in 0.1 M  $\text{Na}_2\text{SO}_4$  solution is only 50% of that in air, and its elongation decreased to 1/4 of the value in air. These results indicated that the magnesium alloy is very sensitive for interaction between corrosive environment and mechanical force. The time to fracture, elongation to fracture and reduction of area of the specimens decrease dramatically (10%) compared to those in air.

## 4. Summary

The phenomenological results of the formation, spreading of micro-droplets and transformation of micro-droplets into a thin water film on pure magnesium and as-cast AZ91 magnesium alloy during cyclic wet-dry condition confirmed that the addition of Al changed the hydrophilicity of the alloy, which is one of the reasons that AZ91 alloy had better corrosion resistance. The grain boundary and  $\beta$  phase for AZ91 magnesium alloy had no influences on the formation and spreading of micro-droplets. The corrosion product simulated the formation and spreading of micro-droplets due to the special structure of the corrosion product.

In solution, when the immersion time was short, the corrosion product can not completely form on the whole surface, and film coverage rate and the metastable  $\text{Mg}^+$

concentration controlled the corrosion process of AZ91 alloy. With the increasing immersion time, the main corrosion products were hydroxides and sulfates. The corrosion process of AZ91 alloy was mainly dominated by the film coverage rate. When the immersion time was more than 181h, localized corrosion occurred on the surface and developed in transverse and depth. At this stage, the corrosion process of matrix was controlled by three surface state variables: the area fraction  $\mathcal{S}_1$  of the region controlled by the formation of  $\text{Mg}(\text{OH})_2$ , the area fraction  $\mathcal{S}_2$  of the region controlled by the precipitation of  $\text{MgAl}_2(\text{SO}_4)_4 \cdot 2\text{H}_2\text{O}$ , and the metastable  $\text{Mg}^+$  concentration  $C_m$ .

Increasing the temperature and relative humidity has a detrimental effect on the fatigue crack growth rate of AZ61. FCP rate increases remarkably with increasing temperature and relative humidity. Fatigue of Magnesium alloys at elevated temperatures is a creep fatigue. Water vapor improved the  $m$  value of Paris equation. Hydrogen embrittlement may be primarily responsible for accelerating FCP rate in humid air. AlMn particles speed FCP rate of Mg alloys.

The fatigue lifetime of rolled AZ31B decreased with the increase of chloride ion concentration of the solutions. AE data shows that after crack initiation, crack had a fairly long stable propagation stage and came into rapid propagation at last stage. AE energy can primely express the experienced damage of the material.

Magnesium alloy is very sensitive for the interaction between corrosive environment and mechanical force.

### Acknowledgements

The authors acknowledge the financial support by the Hundred Talent Project and the National Science Foundation of China. Our graduate students, Mr. Jian Chen, Mr. Rongchang Zeng, and Mr. Huamao Zhou's hard work in laboratory are appreciated.

### References

1. G. L. Makar and J. Kruger, *Inter. Mater. Rev.*, **38**, 138 (1993).
2. J. D. Hanawalt, C. E. Nelson, and J. A. Peloubet, *Trans. Am. Inst. Mining Met. Eng.*, **147**, 273 (1942).
3. S. Mathieu, C. Rapin, J. Steinmetz, and P. Steinmetz, *Corros. Sci.*, **45**, 2741 (2003).
4. R. Ambat, N. N. Aung, and W. Zhou, *Corros. Sci.*, **42**, 1433 (2000).
5. N. LeBozec, M. Jonsson, and D. Thierry, *Corrosion* **60**, 356 (2004).
6. J. H. Nordin, S. Ono, N. Masuko, and K. Nisancioglu, *J. Electrochem. Soc.*, **142**, 3320 (1995).
7. P. Schmutz, V. Guillaumin, R. S. Lillard, J. A. Lillard, and G. S. Frankel, *J. Electrochem. Soc.*, **150**, B99 (2003).
8. G. Baril and N. Pebere, *Corros. Sci.*, **43**, 471 (2001).
9. G. Baril, C. Blanc, and N. Pebere, *J. Electrochem. Soc.*, **148**, B489 (2001).
10. N. Pebere, C. Riera, and F. Dabosi, *Electrochim. Acta*, **35**, 555 (1990).
11. G. Song, A. Atrens, X. Wu, and B. Zhang, *Corros. Sci.*, **40**, 1769 (1998).
12. G. Song, A. Atrens, and M. Dargusch, *Corros. Sci.*, **41**, 249 (1999).
13. O. Lunder, J. E. Lein, T. Kr. Aune, and K. Nisancioglu, *Corrosion*, **45**, 741 (1989).
14. L. Fairman and H. Bray, *Corros. Sci.*, **5**, 711 (1965).
15. G. Song, A. Atrens, D. John, X. Wu, and J. Nairn, *Corros. Sci.*, **39**, 1981 (1997).
16. A. Eliezer, E. M. Gutman, E. Abramov, and Ya. Unigovski, *Journal of Light Metals*, **1**, 179 (2001).
17. Ya. Unigovski, A. Eliezer, E. Abramov, Y. Snir, and E. M. Gutman, *Materials Science and Engineering A*, **360**, 132 (2003).
18. R. G. Song, C. Blawert, W. Dietzel, and A. Atrens, *Materials Science and Engineering: A*, **39**, 308 (2005).
19. Jian Chen, Jianqiu Wang, Enhou Han, and Wei Ke, *Corrosion Science*, **49**, 1625 (2007).
20. Jian Chen, Jianqiu Wang, Enhou Han, and Wei Ke, *Material Sciences Forum*, **546**, 537 (2007).
21. Jian Chen, Jianqiu Wang, Enhou Han, and Wei Ke, *Electrochim. Acta*, **52**, 3299 (2007).
22. Jian Chen, Jianqiu Wang, Enhou Han, Junhua Dong, and Wei Ke, *Material and Corrosion*, **57**, 789 (2006).
23. Rongchang Zeng, Enhou Han, and Wei Ke, *Material Sciences Forum*, **546**, 409 (2007).
24. Huamao Zhou, Jianqiu Wang, Qishan Zang, Enhou Han, and Wei Ke, *Material Sciences Forum*, **546**, 579 (2007).
25. C. M. Houston, *Eng Fracture Mech.*, **8**, 315 (1976).